*International Conference on Mathematics, Computational Methods & Reactor Physics (M&C 2009)*
Saratoga Springs, New York, May 3-7, 2009, on CD-ROM, American Nuclear Society, LaGrange Park, IL (2009)

# TIME-STEP LIMITS FOR A MONTE CARLO COMPTON-SCATTERING METHOD

**Jeffery D. Densmore, James S. Warsa, and Robert B. Lowrie**
Computational Physics and Methods Group, Los Alamos National Laboratory
P.O. Box 1663, MS D409, Los Alamos, NM 87545, USA
jdd@lanl.gov; warsa@lanl.gov; lowrie@lanl.gov

## ABSTRACT

We perform a stability analysis of a Monte Carlo method for simulating the Compton scattering of photons by free electron in high energy density applications and develop time-step limits that avoid unstable and oscillatory solutions. Implementing this Monte Carlo technique in multiphysics problems typically requires evaluating the material temperature at its beginning-of-time-step value, which can lead to this undesirable behavior. With a set of numerical examples, we demonstrate the efficacy of our time-step limits.

*Key Words:* Radiative transfer; Monte Carlo; Compton scattering; Stability analysis; Time-step limit

## 1. INTRODUCTION

Compton scattering is an important aspect of radiative transfer in high energy density applications [1]. In this process, the frequency and direction of a photon are altered by colliding with a free electron. The change in frequency of a scattered photon results in an energy exchange between the photon and target electron and energy coupling between radiation and matter. Canfield, Howard, and Liang have presented a Monte Carlo method for simulating Compton scattering that models the photon-electron collision kinematics exactly [2]. However, implementing their technique in multiphysics problems that include the effects of radiation-matter energy coupling typically requires evaluating the material temperature at its beginning-of-time-step value. This explicit evaluation can lead to unstable and oscillatory solutions.

In this paper, we perform a stability analysis of this Monte Carlo method and present time-step limits that avoid instabilities and nonphysical oscillations by considering a spatially independent, purely scattering radiative-transfer problem. Examining a simplified problem is justified because it isolates the effects of Compton scattering and existing Monte Carlo techniques can robustly model other physics [3, 4] (such as absorption, emission, sources, and photon streaming). Our analysis begins by simplifying the equations that are solved via Monte Carlo within each time step using the Fokker-Planck approximation [5–8]. Next, we linearize these approximate equations about an equilibrium solution such that the resulting linearized equations describe perturbations about this equilibrium. We then solve these linearized equations over a time step and determine the corresponding eigenvalues, quantities that can predict the behavior of solutions generated by a Monte Carlo simulation as a function of time-step size and other physical parameters. With these results, we develop our time-step limits. This approach is similar to our recent investigation of time discretizations for the Compton-scattering Fokker-Planck equation [9–11].

We begin the remainder of this paper by presenting our simplified radiative-transfer problem and reviewing the Monte Carlo method for simulating Compton scattering. We then perform a stability analysis of this Monte Carlo technique, an investigation that we follow by developing our time-step limits. Next, we demonstrate the effectiveness of these time-step limits using a set of numerical examples. We conclude with a brief discussion.

## 2. RADIATIVE TRANSFER, COMPTON SCATTERING, AND MONTE CARLO

The specific radiative-transfer problem we examine is described by [1]

$$\frac{1}{c}\frac{\partial I}{\partial t} + \sigma_s I = \int\int \frac{\nu}{\nu'}\sigma_s(\nu' \rightarrow \nu, \mathbf{\Omega}' \cdot \mathbf{\Omega}, T) I(\nu', \mathbf{\Omega}', t) d\nu' d\mathbf{\Omega}' \quad , \tag{1}$$

and

$$\frac{dU}{dt} = \int\int\int\int \left(1 - \frac{\nu}{\nu'}\right) \sigma_s(\nu' \rightarrow \nu, \mathbf{\Omega}' \cdot \mathbf{\Omega}, T) I(\nu', \mathbf{\Omega}', t) d\nu' d\mathbf{\Omega}' d\nu d\mathbf{\Omega} \quad . \tag{2}$$

Here, $\nu$ is the photon frequency, $\mathbf{\Omega}$ is the angular variable, $t$ is the temporal variable, $I(\nu, \mathbf{\Omega}, t)$ is the radiation intensity, $T(t)$ is the material temperature, $\sigma_s(\nu, T)$ is the total scattering opacity, $\sigma_s(\nu' \rightarrow \nu, \mathbf{\Omega}' \cdot \mathbf{\Omega}, T)$ is the differential scattering opacity, and $c$ is the speed of light. In addition, the material energy density $U(T)$ is related to the material temperature through

$$\frac{dU}{dT} = C_v \quad , \tag{3}$$

where $C_v(T)$ is the heat capacity. Note that we have neglected induced scattering in Eqs. (1) and (2), a physical effect that would make these expressions nonlinear functions of the radiation intensity.

The differential scattering opacity, which models Compton scattering, has a complicated dependence on the material temperature [1],

$$\sigma_s(\nu' \rightarrow \nu, \mathbf{\Omega}' \cdot \mathbf{\Omega}, T) = N_e \int \sqrt{1 - |\mathbf{v}|^2/c^2} \frac{1 - \mathbf{\Omega}' \cdot \mathbf{v}/c}{1 - \mathbf{\Omega} \cdot \mathbf{v}/c} \mu_{\text{KN}}(\nu_0' \rightarrow \nu_0, \mathbf{\Omega}_0' \cdot \mathbf{\Omega}_0) f(\mathbf{v}, T) d\mathbf{v} \quad . \tag{4}$$

In this expression, $N_e$ is the electron density, $\mathbf{v}$ is the electron velocity, $\mu_{\text{KN}}(\nu_0' \rightarrow \nu_0, \mathbf{\Omega}_0' \cdot \mathbf{\Omega}_0)$ is the Klein-Nishina electron rest-frame differential scattering cross section, and $f(\mathbf{v}, T)$ is the relativistic Maxwellian electron-velocity distribution. The subscript $0$ denotes photon properties in the electron rest frame. For a given value of the electron velocity, these rest-frame properties can be related to their laboratory-frame counterparts with a Lorentz transformation [1, 12]. The total scattering opacity is simply the differential scattering opacity integrated over all outgoing frequencies and directions,

$$\sigma_s(\nu, T) = \int\int \sigma_s(\nu \rightarrow \nu', \mathbf{\Omega} \cdot \mathbf{\Omega}', T) d\nu' d\mathbf{\Omega}' \quad . \tag{5}$$

Two quantities of interest based on the radiation intensity are the spectral radiation energy density,

$$E(\nu, t) = \frac{1}{c} \int I(\nu, \mathbf{\Omega}, t) d\mathbf{\Omega} \quad , \tag{6}$$

and the total radiation energy density,

$$\begin{aligned}\mathcal{E}(t) &= \frac{1}{c}\int\int I(\nu,\mathbf{\Omega},t)d\mathbf{\Omega}d\nu \\ &= \int E(\nu,t)d\nu \quad .\end{aligned} \tag{7}$$

Because we have not included absorption, emission, or induced scattering in Eqs. (1) and (2), the equilibrium spectral radiation energy density in this case is a Wien distribution:

$$W(\nu,T) = \frac{hN_p}{2}\left(\frac{h\nu}{kT}\right)^3 e^{-h\nu/kT} \quad . \tag{8}$$

Here, $N_p$ is the photon density. Substituting Eq. (8) into Eq. (7) yields the total radiation energy density corresponding to a Wien distribution,

$$\mathcal{E}(T) = 3kTN_p \quad . \tag{9}$$

We can define a radiation heat capacity in a manner similar to Eq. (3) by taking the temperature derivative of Eq. (9),

$$C_r = \frac{d\mathcal{E}}{dT} = 3kN_p \quad . \tag{10}$$

To solve Eqs. (1) and (2) using Monte Carlo, we first prescribe a temporal grid $0 = t_0 < t_1 < t_2 < \cdots$. Then, within each time step $t_n < t \leq t_{n+1}$, we explicitly approximate the temperature dependence of the total and differential scattering opacities and write Eqs. (1) and (2) as

$$\frac{1}{c}\frac{\partial I}{\partial t} + \sigma_{s,n}I = \int\int \frac{\nu}{\nu'}\sigma_s(\nu' \rightarrow \nu, \mathbf{\Omega}'\cdot\mathbf{\Omega}, T_n)I(\nu',\mathbf{\Omega}',t)d\nu' d\mathbf{\Omega}' \quad , \tag{11}$$

and

$$\begin{aligned}&U_{n+1} - U_n \\ &\quad = \int_{t_n}^{t_{n+1}}\int\int\int\int \left(1 - \frac{\nu}{\nu'}\right)\sigma_s(\nu' \rightarrow \nu, \mathbf{\Omega}'\cdot\mathbf{\Omega}, T_n)I(\nu',\mathbf{\Omega}',t)d\nu' d\mathbf{\Omega}' d\nu d\mathbf{\Omega} dt \quad .\end{aligned} \tag{12}$$

where the subscript $n$ denotes quantities evaluated at time $t_n$. For each time step, we can determine the radiation intensity from Eq. (11) with standard Monte Carlo methods. When a particle scatters, its new frequency and direction are calculated as follows [2]:

1. sample a tentative target electron velocity
2. Lorentz transform the incident frequency and direction to the electron rest frame
3. accept the target electron velocity based on the value of the Klein-Nishina total scattering cross section (i.e., the Klein-Nishina differential scattering cross section integrated over all outgoing frequencies and directions)
4. determine the outgoing frequency and direction in the electron rest frame according to the Klein-Nishina differential scattering cross section

5. Lorentz transform the outgoing frequency and direction back to the laboratory frame

The fourth step can be performed using existing techniques [13, 14]. In the first step, the electron velocity is sampled from the temperature-dependent distribution $f(\mathbf{v}, T)$, the same distribution that carries the temperature dependence of the total and differential scattering opacities. Because this distribution must be fully specified before the Monte Carlo simulation begins, we employ the beginning-of-time-step value of the material temperature to process scattering events; for this reason, we have expressed the total and differential scattering opacities in Eqs. (11) and (12) with an explicitly evaluated material temperature. At the end of each time step, we can update the material temperature through Eqs. (3) and (12).

## 3. STABILITY ANALYSIS

We begin our stability analysis by simplifying Eqs. (11) and (12) using the Fokker-Planck approximation [5–8],

$$\frac{1}{\sigma_{\text{Th}} c}\frac{\partial E}{\partial t} = \nu\frac{\partial}{\partial \nu}\left[\nu\frac{kT_n}{mc^2}\frac{\partial E}{\partial \nu} + \left(\frac{h\nu}{mc^2} - 3\frac{kT_n}{mc^2}\right)E\right] \quad , \tag{13}$$

and

$$\begin{aligned} U_{n+1} - U_n &= -\sigma_{\text{Th}} c \int_{t_n}^{t_{n+1}} \int \nu\frac{\partial}{\partial \nu}\left[\nu\frac{kT_n}{mc^2}\frac{\partial E}{\partial \nu} + \left(\frac{h\nu}{mc^2} - 3\frac{kT_n}{mc^2}\right)E\right] d\nu dt \\ &= -\int (E_{n+1} - E_n) d\nu \quad . \end{aligned} \tag{14}$$

Note that the second equality in Eq. (14) follows from Eq. (13). In these expressions, $k$ is Boltzmann's constant, $h$ is Planck's constant, $mc^2$ is the electron rest mass in energy units, and $\sigma_{\text{Th}}$ is the Thomson opacity, a quantity that is independent of photon frequency and material temperature but directly proportional to the electron density. The Fokker-Planck approximation is valid when the photon frequency and material temperature are small with respect to the electron rest mass, i.e.,

$$\frac{h\nu}{mc^2} \ll 1 \quad \text{and} \quad \frac{kT}{mc^2} \ll 1 \quad . \tag{15}$$

Although these conditions are not always satisfied, we are only using this approximation to generate time-step limits, not actual solutions.

Next, we linearize Eqs. (13) and (14) by first expressing the material temperature and spectral radiation energy density as

$$T_n = T + \delta T_n \quad , \tag{16}$$

and

$$E(\nu, t) = W(\nu, T) + \delta E(\nu, t) \quad . \tag{17}$$

Here, $\delta T_n$ and $\delta E$ are (ideally small) perturbations in the material temperature and spectral radiation energy density, respectively, about their equilibrium values, and $T$ is now the

equilibrium material temperature. When we substitute Eqs. (16) and (17) into Eq. (13), ignore terms of order $O(\delta T_n \delta E)$, and make use of Eq. (8), we have

$$\frac{1}{\sigma_{\text{Th}} c}\frac{\partial}{\partial t}\delta E = \nu\frac{\partial}{\partial \nu}\left[\nu\frac{kT}{mc^2}\frac{\partial}{\partial \nu}\delta E + \left(\frac{h\nu}{mc^2} - 3\frac{kT}{mc^2}\right)\delta E\right] + \frac{hN_p}{2}\frac{k\delta T_n}{mc^2}\left[\left(\frac{h\nu}{kT}\right)^5 - 4\left(\frac{h\nu}{kT}\right)^4\right]e^{-h\nu/kT} \quad , \tag{18}$$

which is the linearized version of Eq. (13). In addition, evaluating Eq. (14) with Eqs. (16) and (17) yields

$$U(T + \delta T_{n+1}) + \int E_{n+1} d\nu = U(T + \delta T_n) + \int E_n d\nu \quad . \tag{19}$$

If we expand $U(T + \delta T_n)$ in a Taylor series about $T$, apply Eq. (3), and ignore terms of $O(\delta T_n^2)$, we can write

$$\begin{aligned} U(T + \delta T_n) &= U(T) + \delta T_n \frac{dU}{dT} + O\left(\delta T_n^2\right) \\ &\approx U(T) + C_v(T)\delta T_n \quad . \end{aligned} \tag{20}$$

Combining Eqs. (19) and (20) gives the linearized version of Eq. (14),

$$C_v(T)\delta T_{n+1} + \int E_{n+1} d\nu = C_v(T)\delta T_n + \int E_n d\nu \quad . \tag{21}$$

For more details regarding this linearization process, see Ref. [11].

We can simplify Eqs. (18) and (21) by defining the following dimensionless transformations:

$$\frac{h\nu}{kT} \rightarrow x \quad ; \tag{22}$$

$$\frac{kT}{mc^2}\sigma_{\text{Th}} ct \rightarrow t \quad ; \tag{23}$$

$$\frac{\delta E(\nu, t)}{hN_p} \rightarrow \delta E(x, t) \quad ; \tag{24}$$

$$\frac{\delta T_n}{T} \rightarrow \delta T_n \quad ; \tag{25}$$

$$\frac{C_v(T)}{kN_p} \rightarrow C_v \quad . \tag{26}$$

Note that $x$ represents a nondimensional frequency. Using Eqs. (22)–(26) allows us to express Eqs. (18) and (21) as

$$\frac{\partial}{\partial t}\delta E = M\delta E + \delta T_n F \quad , \tag{27}$$

and

$$C_v \delta T_{n+1} + \int_0^\infty \delta E_{n+1} dx = C_v \delta T_n + \int_0^\infty \delta E_n dx \quad , \tag{28}$$

where it is understood that all quantities are dimensionless. In Eq. (27), $M$ is the nondimensional Fokker-Planck operator,

$$M\delta E = x^2\frac{\partial^2}{\partial x^2}\delta E + x(x-2)\frac{\partial}{\partial x}\delta E + x\delta E \quad , \tag{29}$$

and

$$F(x) = \frac{1}{2}(x^5 - 4x^4)e^{-x} \quad . \tag{30}$$

Our analysis continues by solving Eqs. (27) and (28) over a time step. To represent the frequency dependence of $\delta E$, we employ an expansion based on the eigenfunctions of $M$. The eigenvalue problem of interest is then

$$My_\lambda + \lambda y_\lambda = 0 \quad . \tag{31}$$

Here, $y_\lambda(x)$ is an eigenfunction of $M$ and $\lambda$ is the corresponding eigenvalue. Kompaneets [5] and Pomraning [15] have shown that the solution to Eq. (31) consists of two discrete eigenfunction-eigenvalue pairs,

$$y_0(x) = \frac{1}{\sqrt{2}}x^3e^{-x} \quad , \quad \lambda = 0 \quad , \tag{32}$$

and

$$y_2(x) = \frac{1}{\sqrt{2}}(x^3 - 2x^2)e^{-x} \quad , \quad \lambda = 2 \quad , \tag{33}$$

and a continuum of eigenfunction-eigenvalue pairs,

$$y_\lambda(x) = \sqrt{\frac{\sinh\left[\pi a(\lambda)\right]}{\pi\lambda(\lambda-2)}}x^{3/2+ia(\lambda)}e^{-x}\Psi[-3/2 + ia(\lambda), 1 + 2ia(\lambda); x] \quad , \quad \lambda \geq 9/4 \quad . \tag{34}$$

In Eq. (34), $\Psi$ is the confluent hypergeometric function of the second kind [16] and $a$ is given by

$$a(\lambda) = \sqrt{\lambda - \frac{9}{4}} \quad . \tag{35}$$

Thus, we express $\delta E$ as

$$\delta E = \alpha_0 y_0 + \alpha_2 y_2 + \int_{9/4}^{\infty} \alpha_\lambda y_\lambda d\lambda \quad , \tag{36}$$

where $\alpha_0(t)$, $\alpha_2(t)$, and $\alpha_\lambda(t)$ are time-dependent expansion coefficients that are yet to be determined. A similar expansion of Eq. (30) is [11]

$$F = \sqrt{2}y_2 + \int_{9/4}^{\infty} \beta_\lambda y_\lambda d\lambda \quad , \tag{37}$$

with

$$\beta_\lambda = \frac{\pi}{2}\frac{\lambda^2(\lambda-2)}{\cosh\left[\pi a(\lambda)\right]}\sqrt{\frac{\sinh\left[\pi a(\lambda)\right]}{\pi\lambda(\lambda-2)}} \quad . \tag{38}$$

Substituting Eq. (36) into Eq. (27) and applying Eqs. (31) and (37) and the orthogonality of Eqs. (32)–(34) shows that $\alpha_0$, $\alpha_2$, and $\alpha_\lambda$ must satisfy

$$\frac{d}{dt}\alpha_0 = 0 \quad , \tag{39}$$

$$\frac{d}{dt}\alpha_2 = -2\alpha_2 + \sqrt{2}\delta T_n \quad , \tag{40}$$

$$\frac{d}{dt}\alpha_\lambda = -\lambda\alpha_\lambda + \beta_\lambda \delta T_n \quad . \tag{41}$$

When we solve Eqs. (39)–(41), we see that the end-of-time-step values of these expansion coefficients are related to their beginning-of-time-step counterparts by

$$\alpha_{0,n+1} = \alpha_{0,n} \quad , \tag{42}$$

$$\alpha_{2,n+1} = \alpha_{2,n}e^{-2\Delta t} + \frac{1}{\sqrt{2}}\left(1 - e^{-2\Delta t}\right)\delta T_n \quad , \tag{43}$$

$$\alpha_{\lambda,n+1} = \alpha_{\lambda,n}e^{-\lambda\Delta t} + \frac{\beta_\lambda}{\lambda}\left(1 - e^{-\lambda\Delta t}\right)\delta T_n \quad . \tag{44}$$

In Eqs. (43) and (44), $\Delta t = t_{n+1} - t_n$ is the time-step size, a quantity that for simplicity we assume is constant. Also, evaluating Eq. (28) using Eq. (36) gives an expression for $\delta T_{n+1}$,

$$C_v(\delta T_{n+1} - \delta T_n) + 3\sqrt{2}(\alpha_{0,n+1} - \alpha_{0,n}) + \sqrt{2}(\alpha_{2,n+1} - \alpha_{2,n}) + \int_{9/4}^{\infty} \frac{2}{\lambda}\beta_\lambda(\alpha_{\lambda,n+1} - \alpha_{\lambda,n})d\lambda = 0 \quad , \tag{45}$$

where the integral of Eq. (34) over frequency is developed in Ref. [11].

We now look for solutions to Eqs. (42)–(45) of the form

$$\alpha_{0,n} = \omega^n \alpha_0 \quad , \tag{46}$$

$$\alpha_{2,n} = \omega^n \alpha_2 \quad , \tag{47}$$

$$\alpha_{\lambda,n} = \omega^n \alpha_\lambda \quad , \tag{48}$$

and

$$\delta T_n = \omega^n \delta T \quad . \tag{49}$$

Here, $\alpha_0$, $\alpha_2$, $\alpha_\lambda$, and $\delta T$ are components of an eigenfunction of Eqs. (42)–(45), while $\omega$ is the corresponding eigenvalue or *amplification factor*. The amplification factor provides insight into the behavior of solutions generated by a particular time discretization as a function of time-step size and other physical parameters. For example, if $|\omega| > 1$, then from Eqs. (46)–(49) the magnitude of the solution can grow without bound and the time discretization is considered unstable. In addition, if $\omega < 0$, then Eqs. (46)–(49) show that the solution can nonphysically oscillate. (We can prove that in our case $\omega$ is real.)

When we substitute Eqs. (46)–(49) into Eqs. (42)–(45), we have

$$(\omega - 1)\alpha_0 = 0 \quad , \tag{50}$$

$$\left(\omega - e^{-2\Delta t}\right)\alpha_2 = \frac{1}{\sqrt{2}}\left(1 - e^{-2\Delta t}\right)\delta T \quad , \tag{51}$$

$$\left(\omega - e^{-\lambda\Delta t}\right)\alpha_\lambda = \frac{\beta_\lambda}{\lambda}\left(1 - e^{-\lambda\Delta t}\right)\delta T \quad , \tag{52}$$

and

$$(\omega - 1)\left(C_v \delta T + 3\sqrt{2}\alpha_0 + \sqrt{2}\alpha_2 + \int_{9/4}^{\infty} \frac{2}{\lambda}\beta_\lambda \alpha_\lambda d\lambda\right) = 0 \quad . \tag{53}$$

Note that the terms in parenthesis on the left sides of Eqs. (50)–(52) are possibly singular. Specifically, we see from Eqs. (50) and (51) that there are discrete singularities at $\omega = 1$ and $\omega = \omega_1$, where

$$\omega_1 = e^{-2\Delta t} \quad . \tag{54}$$

Also, because $\lambda$ varies from $9/4$ to infinity, Eq. (52) shows that there is a continuum of singularities for $0 < \omega \leq \omega_2$, where

$$\omega_2 = e^{-9/4\Delta t} \quad . \tag{55}$$

However, these singularities represent values of $\omega$ that are neither negative nor greater than unity in magnitude and thus cannot cause instabilities or nonphysical oscillations. If we avoid these singularities and any corresponding amplification factors, we can directly solve Eqs. (50)–(52) to write

$$\alpha_0 = 0 \quad , \tag{56}$$

$$\alpha_2 = \frac{1}{\sqrt{2}} \frac{1 - e^{-2\Delta t}}{\omega - e^{-2\Delta t}} \delta T \quad , \tag{57}$$

and

$$\alpha_\lambda = \frac{\beta_\lambda}{\lambda} \frac{1 - e^{-\lambda \Delta t}}{\omega - e^{-\lambda \Delta t}} \delta T \quad . \tag{58}$$

Then, evaluating Eq. (53) with Eqs. (56)–(58) and making use of Eq. (38) allows us to define the characteristic equation for the remaining amplification factors as

$$H(\omega) = 0 \quad , \tag{59}$$

where

$$H(\omega) = C_v + \frac{1 - e^{-2\Delta t}}{\omega - e^{-2\Delta t}} + \frac{\pi}{2} \int_{9/4}^{\infty} \lambda(\lambda - 2) \frac{1 - e^{-\lambda \Delta t}}{\omega - e^{-\lambda \Delta t}} \frac{\tanh\left[\pi a(\lambda)\right]}{\cosh\left[\pi a(\lambda)\right]} d\lambda \quad . \tag{60}$$

An inspection of Eq. (60) reveals that $H$ has the following properties:

$$\lim_{\omega \to \pm\infty} H(\omega) = C_v > 0 \quad ; \tag{61}$$

$$\frac{dH}{d\omega} = -\frac{1 - e^{-2\Delta t}}{(\omega - e^{-2\Delta t})^2} - \frac{\pi}{2} \int_{9/4}^{\infty} \lambda(\lambda - 2) \frac{1 - e^{-\lambda \Delta t}}{(\omega - e^{-\lambda \Delta t})^2} \frac{\tanh\left[\pi a(\lambda)\right]}{\cosh\left[\pi a(\lambda)\right]} d\lambda < 0 \quad . \tag{62}$$

In addition, we see that $H$ diverges to negative infinity as $\omega$ approaches $\omega_1$ from the left and diverges to positive infinity as $\omega$ approaches $\omega_1$ from the right. With these characteristics of $H$, we can predict the locations of solutions to Eq. (59):

1. $\omega \leq 0$: In this region, $H$ monotonically decreases from its asymptotic value of $C_v$ to $H(0)$. Thus, there is a single root if $H(0) \leq 0$. Otherwise, there are no roots.
2. $\omega_2 < \omega < \omega_1$: Here, $H$ monotonically decreases to negative infinity. Thus there is a single root if $H$ is positive near $\omega_2$. Otherwise, there are no roots.

3. $\omega_1 < \omega$: In this region, $H$ monotonically decreases from positive infinity to its asymptotic value of $C_v$. Thus, there are no roots.

Equations (54) and (55) show that if there is a root satisfying $\omega_2 < \omega < \omega_1$, this root is positive and less than unity and cannot cause undesirable behavior. Therefore, only the existence and location of the nonpositive root can predict if the Monte Carlo method described in Section 2 will generate unstable or oscillatory solutions.

In Figure 1, we plot an example of $H$ for specific values of $C_v$ and $\Delta t$. Note that this function is not defined in the shaded region ($0 < \omega \leq \omega_2$) or at $\omega = 1$. Although we have depicted a nonpositive root and a root satisfying $\omega_2 < \omega < \omega_1$, in reality these roots may or may not exist depending on the actual values of $C_v$ and $\Delta t$.

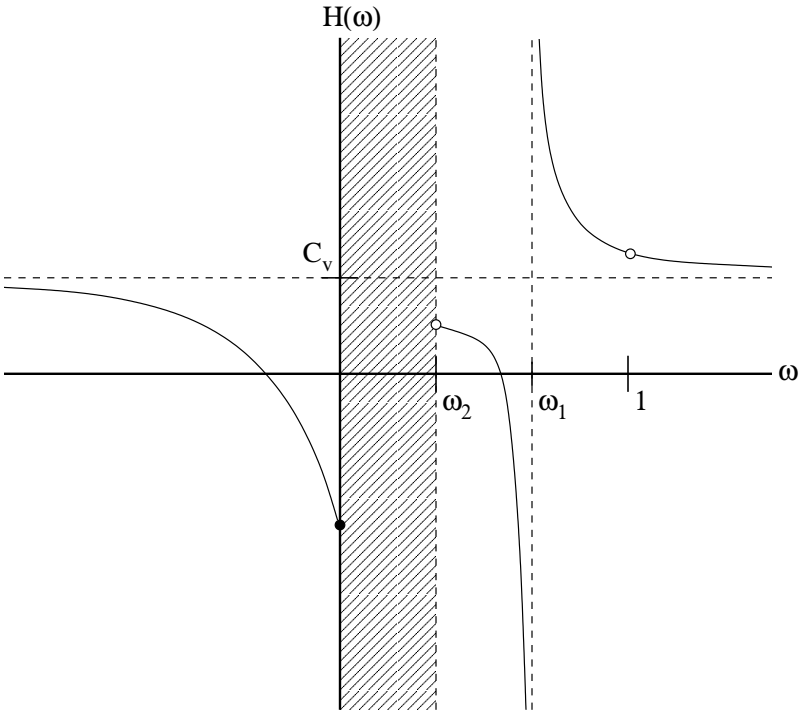


**Figure 1. An Example of $H(\omega)$**

## 4. TIME-STEP LIMITS

We first present a time-step limit that prevents amplification factors less than negative one and the accompanying instabilities. As discussed above, $H$ is a monotonically decreasing function of $\omega$ for $\omega \leq 0$. Thus, we can ensure that there are no roots of Eq. (59) less than negative one by requiring $H$ be non-negative at this value,

$$H(-1) \geq 0 \quad . \tag{63}$$

Combining Eqs. (60) and (63) reveals that the time-step size must satisfy

$$C_v - \frac{1-e^{-2\Delta t}}{1+e^{-2\Delta t}} - \frac{\pi}{2}\int_{9/4}^{\infty} \lambda(\lambda-2)\frac{1-e^{-\lambda\Delta t}}{1+e^{-\lambda\Delta t}}\frac{\tanh\left[\pi a(\lambda)\right]}{\cosh\left[\pi a(\lambda)\right]}d\lambda \geq 0 \quad . \tag{64}$$

We can demonstrate that Eq. (64) is always met regardless of time-step size if

$$C_v \geq 3 \quad . \tag{65}$$

Casting this expression into dimensional units via Eq. (26) yields

$$C_v(T) \geq 3kN_p \quad , \tag{66}$$

or, after applying Eq. (10),

$$C_v(T) \geq C_r \quad . \tag{67}$$

Equation (67) has the interpretation that, when the material heat capacity is larger than the radiation heat capacity, we can expect the material temperature to vary more slowly in time than the radiation intensity, and it is appropriate to explicitly approximate the temperature dependence of the total and differential scattering opacities in Eqs. (11) and (12). If Eq. (67) is not satisfied, we are compelled to solve Eq. (64) numerically for the corresponding time-step limit. This process is most likely impractical. As an alternative, we expand Eq. (64) in a Taylor series about $\Delta t = 0$ to write

$$C_v - 6\Delta t + O(\Delta t^3) \geq 0 \quad . \tag{68}$$

When we transform Eq. (68) into dimensional units through Eqs. (23) and (26), we see that an approximate time-step limit is

$$\Delta t \leq \frac{1}{6}\frac{1}{\sigma_{\text{Th}}}\frac{mc^2}{kT}\frac{C_v(T)}{kN_p} \quad . \tag{69}$$

A more restrictive condition that avoids both unstable *and* oscillatory solutions is to instead prevent negative amplification factors altogether. Analogous to Eq. (63), we require in this case that $H$ is non-negative at zero,

$$H(0) \geq 0 \quad . \tag{70}$$

Substituting Eq. (60) into Eq. (70) shows that the time-step size must now satisfy

$$C_v + 1 - e^{2\Delta t} + \lim_{\omega\to 0^-}\frac{\pi}{2}\int_{9/4}^{\infty} \lambda(\lambda-2)\frac{1-e^{-\lambda\Delta t}}{\omega-e^{-\lambda\Delta t}}\frac{\tanh\left[\pi a(\lambda)\right]}{\cosh\left[\pi a(\lambda)\right]}d\lambda \geq 0 \quad . \tag{71}$$

To determine the actual value of the time-step limit from this expression, we again need a numerical calculation. We can develop an approximate time-step limit by first simplifying Eq. (71) in a manner similar to Eq. (68) as

$$C_v - 12\Delta t - 36\Delta t^2 + O(\Delta t^3) \geq 0 \quad . \tag{72}$$

Then, solving this quadratic equation and casting the results into dimensional units gives

$$\Delta t \leq \frac{1}{6}\frac{1}{\sigma_{\text{Th}}}\frac{mc^2}{kT}\left[\sqrt{1+\frac{C_v(T)}{kN_p}}-1\right] \quad , \tag{73}$$

where we have once again made use of Eq. (23) and (26).

## 5. NUMERICAL RESULTS

We now establish the effectiveness of our time-step limits with two test problems described by Eqs. (1) and (2). In these problems, the (temperature-independent) heat capacity is $C_v = 0.1$ GJ/keV/cm$^3$, the photon density is $N_p = 6.24 \times 10^{23}$ cm$^{-3}$, and the Thomson opacity is $\sigma_{\text{Th}} = 1$ cm$^{-1}$. When we evaluate Eq. (10) using this value of the photon density, we see that the radiation heat capacity is $C_r = 0.3$ GJ/keV/cm$^3$. Thus, for these problem parameters, Eq. (67) indicates that it is possible to observe instabilities for sufficiently large time-step sizes.

To simulate these problems according to the Monte Carlo method discussed in Section 2, we represent the total scattering opacity with a multigroup frequency structure and a frequency and temperature-dependent fit evaluated at group centers that relates the Thomson opacity to the total scattering opacity [17]. We also need the equilibrium material temperature in order to calculate our time-step limits. Combining conservation of energy and Eq. (9) allows us to write

$$U(T) + 3kTN_p = U[T(0)] + \mathcal{E}(0) \quad , \tag{74}$$

where $T(0)$ and $\mathcal{E}(0)$ are the initial material temperature and total radiation energy density, respectively. Equations (3) and (74) form an expression for the equilibrium material temperature. Once this quantity is determined, we can solve Eq. (64), along with Eqs. (23) and (26), for the exact stability time-step limit and evaluate Eq. (69) for the approximate stability time-step limit. A similar process applied to Eqs. (71) and (73) yields the exact and approximate oscillatory time-step limits. Although we report the exact time-step limits for reference, we base our time-step sizes on the approximate time-step limits because they are much easier to calculate and, as we will see, fairly accurate.

In the first problem we examine, the initial material temperature is $1.5$ keV and the initial radiation intensity is isotropic and corresponds to a Wien distribution at $1$ keV. Using these initial conditions shows that the equilibrium material temperature is $1.125$ keV, and the resulting approximate time-step limits are $\Delta t \leq 2.53$ ns to avoid instabilities and $\Delta t \leq 1.05$ ns to prevent nonphysical oscillations. As a comparison, the exact stability time-step limit is $\Delta t \leq 2.82$ ns and the exact oscillatory time-step limit is $\Delta t \leq 1.01$ ns. We simulated this problem with $100{,}000$ particles per time step, $1000$ frequency groups uniformly spaced between $0$ keV and $200$ keV, and time-step sizes of $\Delta t = 1.05$ ns (the approximate oscillatory time-step limit), $2.10$ ns (twice the approximate oscillatory time-step limit), $2.53$ ns (the approximate stability time-step limit), and $5.06$ ns (twice the approximate stability time-step limit). The material temperature generated by these calculations is plotted in Figures 2 and 3. From Figure 2, we see that the material temperature monotonically decreases for $\Delta t = 1.05$ ns and nonphysically oscillates before reaching equilibrium for $\Delta t = 2.10$ ns. In addition, Figure 3 shows that the material temperature again nonphysically oscillates as it moves towards equilibrium for $\Delta t = 2.52$ ns, while further increasing the time-step size to $\Delta t = 5.06$ ns results in an unstable solution that eventually generates a negative material temperature. Of course, this negative material temperature causes the simulation to stop. We conclude that our time-step limits performed as intended for this problem; using the maximum time-step size avoids undesirable behavior (i.e., instabilities for the stability time-step limit and both instabilities and nonphysical oscillations for the oscillatory time-step limit), while doubling the time-step size produces undesirable behavior and demonstrates that our time-step limits are not overly conservative.

The second problem we consider is nearly identical to the first except the initial material temperature is $100$ keV and thus the initial conditions are farther from equilibrium in this case. With these initial conditions, the equilibrium material temperature is $25.75$ keV, and the corresponding approximate time-step limits are $\Delta t \leq 0.110$ ns to prevent instabilities and $\Delta t \leq 0.0457$ ns to avoid nonphysical oscillations. For reference, the exact stability time-step limit is $\Delta t \leq 0.123$ ns and the exact oscillatory time-step limit is $\Delta t \leq 0.0440$ ns. We simulated this problem using $100{,}000$ particles per time step, $200$ frequency groups logarithmically spaced between $0.02$ keV and $2000$ keV, and time-step sizes of $\Delta t = 0.0457$ ns (the approximate oscillatory time-step limit), $0.0914$ ns (twice the approximate oscillatory time-step limit), $0.110$ ns (the approximate stability time-step limit), $0.183$ ns (four times the approximate oscillatory time-step limit), $0.220$ ns (twice the approximate stability time-step limit), and $0.440$ ns (four times the approximate stability time-step limit). The material temperature calculated by these simulations is displayed in Figures 4 and 5. From Figure 4, we see that the material temperature monotonically approaches equilibrium for time-step sizes as large as $\Delta t = 0.110$ ns. Also, Figure 5 shows that the material temperature nonphysically oscillates but eventually reaches equilibrium for $\Delta t = 0.183$ ns and $0.220$ ns. Employing a time-step size of $\Delta t = 0.440$ ns produced a negative material temperature at the end of the first time step instead of an unstable solution, and thus we do not present these results. Again, our time-step limits worked as designed, although they are conservative by a factor of four in this problem as opposed to a factor of two in the first problem.

## 6. CONCLUSIONS

We have performed a stability analysis of a Monte Carlo method for simulating Compton scattering in high energy density applications and have developed time-step limits that avoid unstable and oscillatory solutions. We have demonstrated the efficacy of these time-step limits with a set of numerical examples. In future work, we plan on applying our time-step limits to more complex problems that include the effects of photon streaming, absorption, emission, and sources.

## ACKNOWLEDGMENTS

This work was performed under U.S. government contract DE-AC52-06NA25396 for Los Alamos National Laboratory, which is operated by Los Alamos National Security, LLC, for the U.S. Department of Energy.

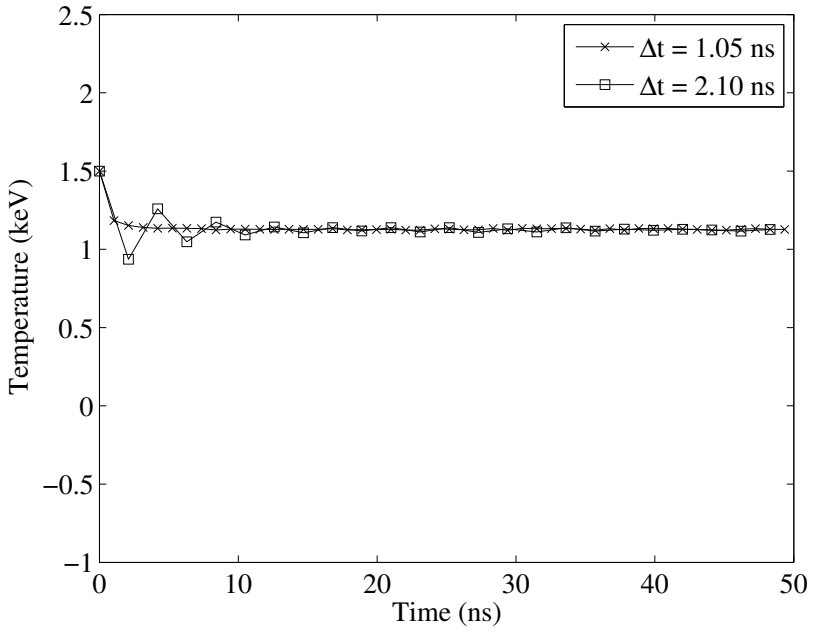


**Figure 2. First Problem Material Temperature for $\Delta t = 1.05$ ns and 2.10 ns**

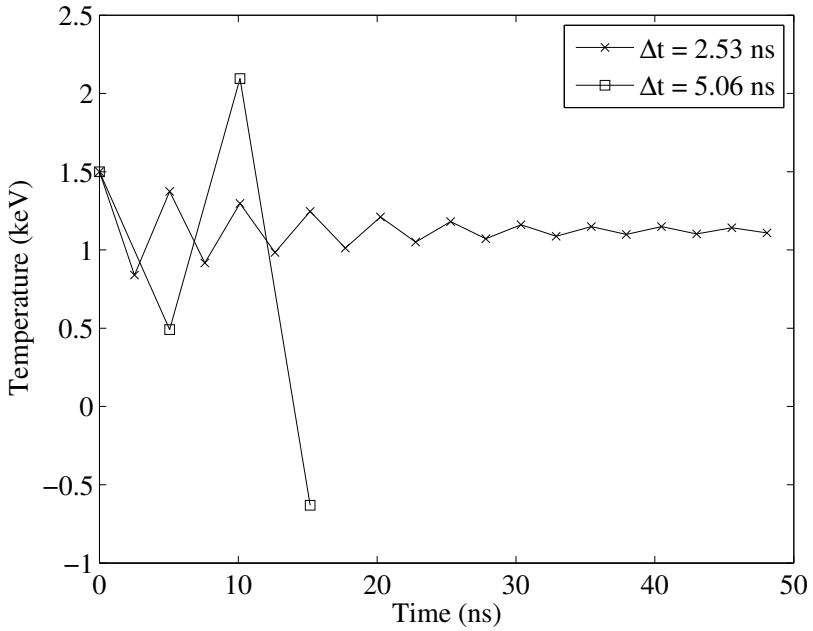


**Figure 3. First Problem Material Temperature for $\Delta t = 2.53$ ns and 5.06 ns**

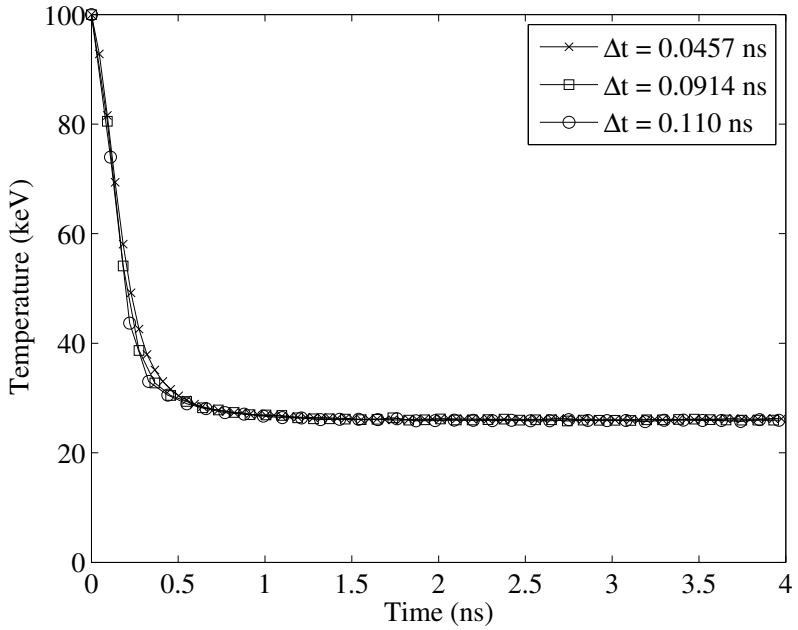


**Figure 4. Second Problem Material Temperature for $\Delta t = 0.0457$ ns, 0.0914 ns, and 0.110 ns**

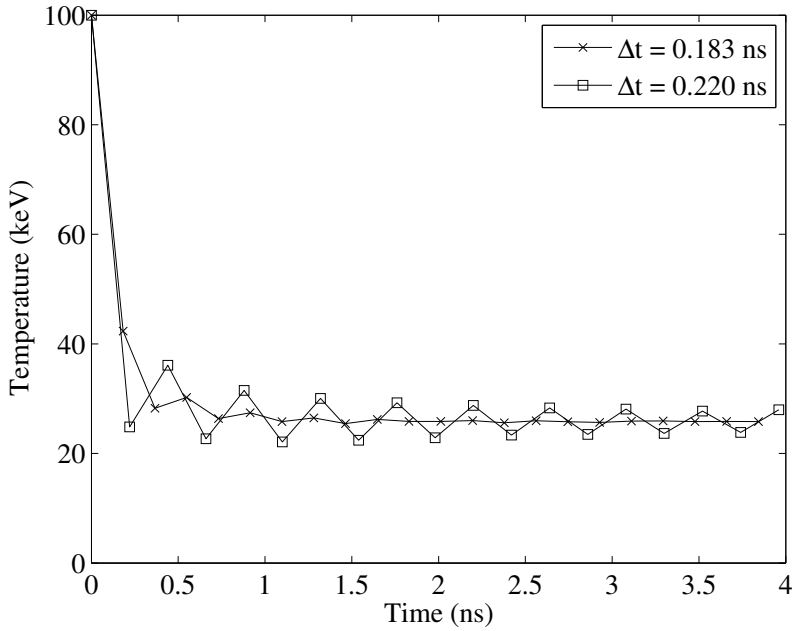


**Figure 5. Second Problem Material Temperature for $\Delta t = 0.183$ ns and 0.220 ns**

## REFERENCES


[1] G.C. Pomraning, *The Equations of Radiation Hydrodynamics*, Pergamon Press, Oxford, United Kingdom (1973).

[2] E. Canfield, W.M. Howard, and E.P. Liang, "Inverse Comptonization by One-Dimensional Relativistic Electrons," *Astrophys. J.*, **323**, 565 (1987).

[3] J.A. Fleck Jr. and J.D. Cummings, "An Implicit Monte Carlo Scheme for Calculating Time and Frequency Dependent Radiation Transport," *J. Comp. Phys.*, **8**, 313 (1971).

[4] T. N'kaoua, "Solution of the Nonlinear Radiative Transfer Equations by a Fully Implicit Matrix Monte Carlo Method Coupled with the Rosseland Diffusion Equation via Domain Decomposition," *SIAM J. Sci. Stat. Comput.*, **12**, 505 (1991).

[5] A.S. Kompaneets, "The Establishment of Thermal Equilibrium between Quanta and Electrons," *Sov. Phys. JETP*, **4**, 730 (1957).

[6] J.I. Katz, *High Energy Astrophysics*, Addison-Wesley Publishing, Menlo Park, California (1987).

[7] G.B. Rybicki and A.P. Lightman, *Radiative Processes in Astrophysics*, WILEY-VCH, Weinheim, Germany (2004).

[8] J.I. Castor, *Radiation Hydrodynamics*, Cambridge University Press, Cambridge, United Kingdom (2004).

[9] J.D. Densmore, J.S. Warsa, and R.B. Lowrie, "Time-Step Limits for a Semi-Implicit Discretization of the Compton-Scattering Fokker-Planck Equation," *Trans. Am. Nucl. Soc.*, **97**, 540 (2007).

[10] J.D. Densmore, J.S. Warsa, R.B. Lowrie, and J.E. Morel, "Linearized Stability Analysis of Two Time Discretizations for the Compton-Scattering Fokker-Planck Equation," *Trans. Am. Nucl. Soc.*, **99**, 328 (2008).

[11] J.D. Densmore, J.S. Warsa, R.B. Lowrie, and J.E. Morel, "Stability Analysis of Implicit Time Discretizations for the Compton-Scattering Fokker-Planck Equation," *J. Comp. Phys.*, submitted.

[12] D. Mihalas and B. Weibel-Mihalas, *Foundations of Radiation Hydrodynamics*, Dover Publications, Mineola, New York (1999).

[13] H. Kahn, "Applications of Monte Carlo," AECU–3259, Rand Corporation (1954).

[14] R.N. Blomquist and E.M. Gelbard, "An Assessment of Existing Klein-Nishina Monte Carlo Sampling Methods," *Nucl. Sci. Eng.*, **83**, 380 (1983).

[15] G.C. Pomraning, "An Eigenfunction Description of Radiative Transfer in Scattering Atmospheres," *Astrophys. J.*, **152**, 809 (1968).

[16] A. Erdélyi, *Higher Transcendental Functions*, Vol. 1, McGraw-Hill Book Company, New York, New York (1953).

[17] B.R. Wienke, "Relativistic Photon-Maxwellian Electron Cross Sections," *Astron. Astrophys.*, **152**, 336 (1985).